

Quantifying the Risk of Wildfire Ignition by Power Lines under Extreme Weather Conditions

Muhammad Waseem, *Student Member, IEEE*, Reza Bayani, *Student Member, IEEE*, Saeed D. Manshadi, *Member, IEEE*, and Hassan Tavakol-Davani

Abstract—This paper presents a surrogate model to quantify the risk of wildfire ignition by individual power lines under extreme weather conditions. Wind speed and wind gust can lead to conductor clashing, which is a cause of igniting disastrous wildfires. The 3D non-linear vibration equations of power lines are employed to generate a dataset that considers physical, structural, and meteorological parameters, including the span of the power line, conductor diameter, wind speed, wind gust, phase clearance, and wind direction. A set of machine learning models is assembled based on these features to generate a score representing the risk of conductor clashing for each power line within a network, quantifying the risk of wildfire ignition. The rendered score represents the chance of the conductor clashing in place of simulating a Runge-Kutta method. A discussion on the impact of various meteorological parameters on power lines under the energization risk is presented. Besides, it is shown how the presented risk measure can be utilized to weigh in the fire safety and service continuity trade-off.

Index Terms—wildfire, power system resilience, risk quantification, surrogate models, weather conditions.

I. INTRODUCTION

A. Motivation

Wildfires are among threats that could potentially lead to disastrous events throughout the world. Arguably, fire seasons are getting more prolonged and more frequent, primarily due to climate change and global warming [1]. The fire frequency and the burnt area in the western U.S. have grown exponentially since 1950 [2]. The 2018 California wildfires resulted in capital losses of \$27.7 billion, health costs of \$32.2 billion, and indirect losses of \$88.6 billion, and thus total loss of \$148.5 billion [3]. Faults within power lines are counted among causes for fire ignition. Fires caused by power lines account for almost half of the most destructive fires in California history [4]. Pacific Gas & Electric Company (PG&E) declared 414 fire ignition events during 2015-2017 caused by electric power lines [5]. Extreme winds, such as the ones occurring during fall seasons in Southern California, not only increase the risk of power line-related ignitions but also facilitate the propagation of fire. According to the historical data during the period 1960-2009 in Southern California, fires ignited by power lines burn on average ten times the area burnt as a result of fires initiated by other sources [6]. Conductor clashing (phase to phase faults), fall of the line on the ground

(phase to ground faults), arcs, and contact with the surrounding vegetation are among the incidents related to power lines that could cause ignitions [7].

In addition to the wind, temperature, humidity, and vegetation are among the meteorological and geographical factors correlated, with the chances of fire ignitions by power lines [8], [9] with wind as the leading factor. Although low wind speeds will cool off conductors and can benefit dynamic line rating [10], high wind speeds can lead to faults within power lines. According to the analysis of the 11-years outage record data provided by San Diego Gas & Electric (SDG&E), for every 25 km/h increase in the wind gust speed, the outage probability is increased ten times [6]. Higher wind speeds are associated with higher chances of fire ignition. For example in California's 2003 Cedar fire and October 2007 firestorms, almost no power line-related fire ignitions were attributed to 2003 fires. In contrast, nearly half of the fires (9 out of 20) in October 2007 were initiated by power lines. The difference is because the peak wind speeds during 2007 were 80% higher than those during 2003 [6].

High sustained wind speeds (average wind speed lasting over 10 minutes) typically occur during California's late summer and fall seasons. Even though the mechanical design standards of overhead power lines anticipate windy conditions, temporarily lasting wind gusts (1-20 seconds) could outweigh these considerations. The wind speed and wind gust could significantly affect the swing angle of the conductors [11]. The combination of high sustained wind speeds and wind gusts could lead to conductor clashing, which, together with hot and dry weather conditions, highly increases the risk of wildfires taking place. The energized power line conductors clashing may cause vaporization and melting of the conductor materials and ejection of the molten metal as small particles [12]. Drop of hot particles due to conductor clashing on dried vegetation or direct contact between conductors and vegetation can potentially ignite wildfires [13]–[15]. Thus, the dead, dying, and diseased trees near the power lines elevate the wildfire risk, mainly when conductor clashing occurs. The combustible vegetation in a 100 feet radius around the power network is typically considered a risk to create the fire [16]. However, the wildfire will not happen if there is no ignition in the first place. That is why utilities across California adopted *Public Safety Power Shut-offs* (PSPS) to avoid such ignitions under extreme weather conditions with wind gusts exceeding 22.8 m/s.

California Public Utilities Commission allows utilities to deliberately cut off power to electrical lines as a

M. Waseem, Reza Bayani, and S. D. Manshadi are with Department of Electrical and Computer Engineering, San Diego State University, San Diego, CA, 92182, USA email:(mwaseem2282@sdsu.edu; rbayani@sdsu.edu; smanshadi@sdsu.edu)

Hassan Tavakol-Davani is with Department of Civil, Construction, and Environmental Engineering, San Diego State University, San Diego, CA, 92182, USA email:(htavakol@sdsu.edu)

preventive measure in high-risk situations with a looming threat of wildfire ignition [4]. From 2013 to 2020, PG&E, SDG&E, Southern California Edison, and PacifiCorp collectively performed 51 PSPS events in multiple locations within California (Saddle Ridge, Tick in Los Angeles, Caples in El Dorado, etc.), which impacted 3.2 million customers [17]. However, a PSPS event has its risks and unfavorable consequences, particularly for medically vulnerable populations and low-income communities [4], [8]. In October 2019, PSPS events by PG&E affected 1.8 million customers, with outages lasting more than five days in some cases. It is estimated that PSPS events could cost the California economy in order of billions [18] and casualties due to lack of power supply [19]. It can be concluded that although PSPS events are a practical and proactive approach for wildfire risk reduction, they could *impose unnecessary difficulties if blanket outages are performed throughout a power grid within a region*. In this work, we propose a method that can pinpoint the segments of the network with higher fire ignition risk, which could help PSPS events be targeted towards those lines of the grid instead of an entire section of the grid.

With the increase in the availability of meteorological sensing data and estimation techniques with high granularity, this paper aims to present a scientific machine learning setup for a surrogate model that can quantify the potentially disastrous impacts of extreme wind events on the clashing of conductors on each power line. In order to do so, we propose a machine learning-based model that is able to instantly predict the risk of wildfire ignition for each line of the power system. Also, we present a scoring system that can predict the conductor-clashing probability of a power line based on the real-time wind speed data. The resulting score can be used to determine precisely which sections and lines of the grid should be subject to PSPS, consequently minimizing the area and population impacted by unnecessary outages. The procured quantified measure will pave the way to render operational planning models for power grids within the areas under the risk of wildfire. With the availability of appropriate data, our metric could be generalized to include the ignition risks imposed by falling off the poles and power lines on the ground and falling of the trees on the power lines as well. Our approach could also be generalized to account for other meteorological measurements, including but not limited to humidity and temperature.

B. Literature Review

In addition to wind speed, other factors also impact the risk of wildfire ignition during extreme weather conditions, including ambient temperature, conductor spacing, and the weight of the conductor. The variations in ambient temperature due to the wind are examined in [20]. The authors in [9] developed a fire hazard prevention system based on meteorological factors, including relative humidity, average daily precipitation, daily average temperature, and daily extreme wind speed. However, it is not clear how the data is modeled to forecast hazards or the scope of preventive measures. An experiment to investigate the minimum spacing

required among the conductors is performed in [21], but other factors are left out of the study.

Studies are dedicated to the long-term impact of high wind speed on the failure probability. Still, none of them considered quantifying the wildfire risk if the lines are energized given a specific weather condition with wind gusts. The difference between the measured and theoretical wind loads on the power lines are examined in [22], and the wind adjustment factor using the collected data is also studied. However, this study ignored the effect of strong wind gusts. A two-stage forecast method is proposed in [23] to enable grid operators with a classification tool for different wind types. The first stage creates empirical models using weather and historical data. The second stage considers the real-time tracking of high winds. The wind direction also impacts the possibility of the conductor clashing under extreme weather conditions. The smaller angle between the line and wind leads to greater failure probability [24].

A review of the electricity grid vulnerabilities amid natural disasters, including wildfires, is presented in [25]. There are some recent attempts to facilitate operational planning of the electricity grid, including the risk of a wildfire [26]. The short-term operation of the system *during wildfire* given the thermal effects of wildfires on the dynamic rating of power lines is given in [27]. An optimization framework to balance the wildfire risk and power shut-off within impacted areas is presented in [28], but it does not quantify the operation risk of each line. The fire ignition score due to high impedance faults through contact with vegetation is calculated in [29], while it requires the ignition event to occur first. The probability of wildfire ignition is computed in [30], but it only considered the wind speed. As suggested in a review article on wildfire risk management in power grids [31], there is a lack of research on wildfire prediction when power grid infrastructures cause the fire.

A gap in assessing the impact of meteorological conditions on power lines using a physical model and building a scoring mechanism to quantify the probability of conductors clashing exists in the literature. This paper aims to fill this gap by presenting a surrogate model that can efficiently quantify the risk of wildfire ignition under extreme weather conditions considering the wind speed, wind gust, wind direction, and the structure of the power lines, including span, conductor diameter, and phase clearance.

C. Summary of the Contributions

The contributions of this paper are outlined as follows:

- 1) A method for quantifying the risk of power line conductor clashing under extreme wind conditions is presented based on a physical model. It will create a scientific foundation to quantify the risk of operation of each specific power line during specific extreme weather conditions.
- 2) A wildfire risk-aware operation planning problem is presented, which incorporates the quantified wildfire hazard risk values. With the availability of the required meteorological data predictions, the proposed formulation

supports decision-makers to decide on the de-energizing of power lines for PSPS events.

- 3) A scoring method is introduced to determine the part of the conductor coming in a clash with the nearby conductors. The predicted score is in the range [0,1), where 0 means no clashing is happening, while 0.99 means the whole conductor except both ends is under clashing. This high-granularity scoring system provides a well-quantified risk of wildfire for each individual power line.
- 4) A comparison of different learning algorithms for predicting the risk of wildfire is performed, and the most accurate model is proposed to predict the conductor-clashing score. The final choice is compared with the nonlinear model and presented a very well performance that can be confidently used as a surrogate model to the original nonlinear model.

II. WILDFIRE RISK AWARE PROBLEM

This section presents the Wildfire Risk Aware operation planning Problem (WRAP) by taking advantage of the quantified risk scores. Applying WRAP to the operation planning of a power system subject to wildfire hazard ensures that the operational constraints of the power system are satisfied. WRAP enables the power system operator to avoid energizing high-risk lines under hazardous conditions. The proposed WRAP formulation is presented in (1), which illustrates how the procured wildfire risk quantification can be utilized in the operational planning problem of power systems.

$$\min_{I, P_d, P_g} \sum_{t \in \mathcal{T}} \left\{ \sum_{l \in \mathcal{L}} K^2 \psi_l^t I_l^t + \sum_{i \in \mathcal{I}} K (P_{i,D}^t - P_{i,d}^t) + \sum_{s \in \mathcal{S}} \sum_{g \in \mathcal{G}} c_g^s P_{g,s}^t \right\} \quad (1a)$$

subject to:

$$\sum_{s \in \mathcal{S}} P_{g,s}^t = P_g^t, \quad \forall g \in \mathcal{G}, \forall t \in \mathcal{T} \quad (1b)$$

$$0 \leq P_{g,s}^t \leq \bar{P}_g^s, \quad \forall g \in \mathcal{G}, \forall s \in \mathcal{S}, \forall t \in \mathcal{T} \quad (1c)$$

$$\sum_{g \in \mathcal{G}_i} P_g^t + \sum_{l \in LT_i} P_l^t = \sum_{l \in LF_i} P_l^t + P_{i,d}^t, \quad \forall i \in \mathcal{I}, \forall t \in \mathcal{T} \quad (1d)$$

$$\underline{P}_g \leq P_g^t \leq \bar{P}_g, \quad \forall g \in \mathcal{G}, \forall t \in \mathcal{T} \quad (1e)$$

$$\alpha P_{i,D}^t \leq P_{i,d}^t \leq P_{i,D}^t, \quad \forall i \in \mathcal{I}, \forall t \in \mathcal{T} \quad (1f)$$

$$-M(1 - I_l^t) + P_l^t \leq \frac{\sum_{i \in B_l^t} \theta_i^t - \sum_{j \in B_l^t} \theta_j^t}{x_l} \leq P_l^t + M(1 - I_l^t), \quad \forall l \in \mathcal{L}, \forall t \in \mathcal{T} \quad (1g)$$

$$-\bar{P}_l \times I_l^t \leq P_l^t \leq \bar{P}_l \times I_l^t, \quad \forall l \in \mathcal{L}, \forall t \in \mathcal{T} \quad (1h)$$

The objective function is presented in (1a), where the summation of the conductor clashing scores, the value of load shedding, and generation cost of units is minimized. The first term in the objective penalizes the operation planning of *energized lines* by a penalty factor K^2 ($K > 1$). Here, the quantified risk value of each line at each time is represented by ψ_l^t , where I_l^t is a binary decision variable denoting the

energization (if 1) or the de-energization (if 0) status of each line at each time, l is the index of lines in the set of power lines \mathcal{L} , and t is the index of time in the set of time steps \mathcal{T} . In the second term of the objective, the operator is penalized if load shedding takes place. Here, $P_{i,D}^t$ is the scheduled consumer demand, and $P_{i,d}^t$ is the amount of demand served at each bus at time, where i is the index of bus in the set of buses \mathcal{I} . The last term in the objective function calculates the generation cost of units based on a piecewise linear function approximation. The output power of each generation unit at each time is divided into different segments denoted by $P_{g,s}^t$, where c_g^s is the generation cost, s is the index of segment of generating units in set \mathcal{S} , and g is the index of generation unit in the set of generation units \mathcal{G} . The sum of power generation of each segment is equal to the total power generation of a unit P_g^t as shown in (1b). The power generation of each segment is constrained to its upper and lower bounds as presented in (1c).

The power flow balance at each node is given in (1d), where P_l^t is power flow of line l at time t . The upper and lower limits of the power generation of each unit at each hour are constrained by (1e). The served demand at each bus is modeled in (1f), where α is a parameter ranging from 0 to 1 and assigns the ratio of the critical demand which must be served. The relationship between the power flow of each power line with the voltage angles of its connecting buses (θ_i^t, θ_j^t) and line reactance (x_l) is presented with two inequalities in (1g), where M is an arbitrarily large number and B_l^t, B_f^t are respectively the set of buses line l is leading to and leaving from. The power line power flow capacity constraint is enforced in (1h), where the thermal capacity is presented by \bar{P}_l . If a line is energized, i.e. $I_l^t = 1$, the inequalities in (1g) become an equality constraint and the thermal limits in (1h) are applied. Conversely if a line is de-energized, i.e. $I_l^t = 0$, the power flow in the line will be zero.

The resulting WRAP formulation in (1) is a mixed-integer linear programming, which can be solved via off-the-shelf solvers. The solution to WRAP will help system operators to balance the risk of wildfire in the operation of the electricity grid under the risk of wildfire. By implementing the quantified risk values of each line at each time in the WRAP, the obtained scheduling of each line's status and the output of generation units guides the system operator in decision making under extreme weather conditions. The procedure for learning a surrogate model that returns the quantified risk values, ψ_l^t , utilized in the formulation is discussed in the upcoming sections.

III. DATA PREPARATION

In this section, the non-linear motion of power lines due to in-plane and out-of-plane vibrations is determined to evaluate the impact of wind on the motion of power lines. A dataset is generated that considers six physical and meteorological features to find the clashing score of each line.

A. Non-linear Equations for Motion of Power Lines

Here, the vibrational model which explains the movement of a power line under wind force is illustrated. We generated

a training dataset that estimates the clashing score of a span within a power line based on this model. In-plane vibrations occur when a power line is in the plane and placed under gravity. Out-of-plane vibrations are perpendicular to the plane above. The spatial configuration of a power line is shown in Fig. 1, where $P(x, t)$, $P(y, t)$, and $P(z, t)$ correspond to the components of external excitation along the x , y , and z -axes, respectively.

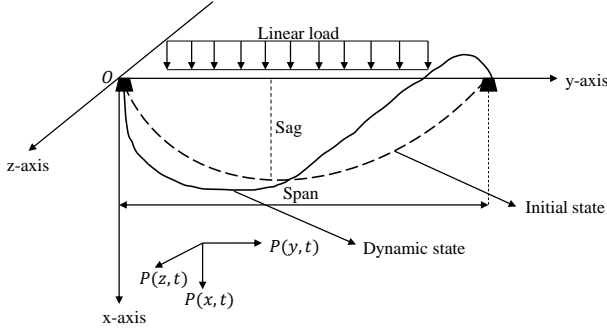


Fig. 1. Spatial configuration of the power line

The 3D geometric non-linear vibration equations of a power line are established using Hamilton's principle [32]. Based on the boundary conditions and modeling assumptions, the 3D equations are simplified to 2D equations. Galerkin's modal truncation method converts 2D continuous partial differential equations to discrete partial differential equations [32]. As shown in (2), the resulting discrete equations represent the coupled in-plane and out-of-plane non-linear motion of the power line. In this paper, the Runge-Kutta method [33] is employed to solve the resulting vibration equations.

$$a_1 \ddot{q}_\nu(t) + a_2 \dot{q}_\nu(t) + a_3 q_\nu^2(t) + a_4 q_\omega^2(t) + a_5 q_\nu^3(t) + a_6 q_\omega^2(t) q_\nu(t) + a_7 \dot{q}_\nu(t) = P_\nu \quad (2a)$$

$$b_1 \ddot{q}_\omega(t) + b_2 \dot{q}_\omega(t) + b_3 q_\nu(t) q_\omega(t) + b_4 q_\nu^2(t) q_\omega(t) + b_5 q_\omega^3(t) + b_6 \dot{q}_\omega(t) = P_\omega \quad (2b)$$

In (2), the governing equations for the generalized coordinates in x and z -axes of a power line, denoted respectively by q_ν and q_ω , are described. Here, P_ν and P_ω represent the external excitation spanning the whole conductor in x and z -axes, respectively. The equations for acquiring P_ν , P_ω , and the parameters $a_1 - a_7$ and $b_1 - b_7$ are given in [32]. The numerical solution of (2) is obtained using a second-order Runge-Kutta method to identify the non-linear vibration characteristics of a power line. The in-plane and out-of-plane responses of the power line using the Galerkin method [34] are represented by $\nu_c(y, t)$ and $\omega_c(y, t)$ respectively and given in (3), where L_c denotes the span of the power line.

$$\nu_c(y, t) = \sin\left(\frac{\pi y}{L_c}\right) \times q_\nu(t) \quad (3a)$$

$$\omega_c(y, t) = \sin\left(\frac{\pi y}{L_c}\right) \times q_\omega(t) \quad (3b)$$

B. Wind Effect on the Motion of Power Lines

A wind gust is a transient increase in wind speed. It occurs when there is an abrupt change from high pressure to low pressure. It is ephemeral in nature and usually lasts for 20 seconds. The discrete wind gust is used to assess the conductor

response to significant wind disturbances. The mathematical representation of discrete wind gust is given in (4).

$$V_{wind} = \begin{cases} 0 & x < 0 \\ \frac{V_m}{2} \left(1 - \cos\left(\frac{\pi x}{d_m}\right)\right) & 0 \leq x \leq d_m \\ V_m & x > d_m \end{cases} \quad (4)$$

Here, V_{wind} is the resultant wind velocity in the power line body axis frame, V_m is the wind gust amplitude, d_m is the length of gust, and x is the traveled distance. The gust length is the range over which the gust builds up, and the gust amplitude represents the increase in wind speed developed by the gust.

The following assumptions are considered for the wind-induced vibrations of a power line.

- 1) The wind load acts in the out-of-plane direction of the power line.
- 2) The wind speed loading effect on the vibrations of power line is considered, but the aerodynamic effects are not considered.

The external excitation due to wind in x -axis direction $P(x, t)$ and z -axis direction $P(z, t)$ are expressed in (5).

$$P(x, t) = 0.5 \rho_a D_c C_D (v_{a-x} - \dot{\nu}_c)^2 \quad (5a)$$

$$P(z, t) = 0.5 \rho_a D_c C_D (v_{a-z} - \dot{\omega}_c)^2 \quad (5b)$$

Here, ρ_a is the density of air, D_c represents power line width facing the wind, C_D represents power line shape factor, v_{a-x} and v_{a-z} represent wind speed along the x and z -axes, respectively. The in-plane and out-of-plane power line vibrational velocities are represented by $\dot{\nu}_c$ and $\dot{\omega}_c$, respectively. Based on the above assumptions, the expressions for a_7 , b_6 , P_ν , and P_ω are updated considering initial values of the state variables and the design hyper-parameters of the power line. Consequently, a new solution is obtained for (2), which incorporates the impact of wind speed on power line motion. Different features and meteorological conditions are included in the model discussed above, such as the span of the power line, conductor diameter, phase clearance, wind speed, wind gust, and wind direction angle. Based on these features, a score ranging from 0 to 1 is obtained, which determines the extent to which the power line is in contact with the neighboring lines.

C. Data Processing and Feature Importance Analysis

Different ranges of each feature based on practical characteristics within the power system are considered to create the training dataset for the surrogate model. The total number of observations in the dataset is 435,600. Table I provides a sample of the generated dataset with scores calculated using the Runge-Kutta method.

Data preprocessing comprises feature selection (dimensions of input data) and feature normalization (normalization of input data). Feature selection ensures that the power line features and meteorological conditions are contributing to predict the score.

It is necessary to quantify the importance of input features to explore the potential improvement in the input data. The input feature importance is calculated using the Gini index of the decision tree algorithm as given in Table II. It is clear that

wind speed and wind gust are among the important leading features, but it is also interesting to observe the impact of span on the clashing score. Although a single important feature cannot capture the thorough relationship between the input and output, it is rational to choose the significant features to predict the conductor-clashing score. Feature normalization is helpful when features of different ranges and scales exist.

TABLE I
DATASET SAMPLE GENERATED USING RUNGE-KUTTA METHOD

Span (ft)	Conductor diameter (mm)	Wind speed (m/s)	Wind gust (m/s)	Phase clearance (ft)	Wind direction (°)	Score [0,1)
600	33.03	10	12	0.5	45	0
800	34.02	18	16	0.5	180	0.01
1000	31.05	28	30	0.5	90	0.12

TABLE II
IMPORTANCE OF INPUT FEATURES

Features	Importance (%)
Wind speed	27.3
Span of line	20.9
Wind gust	13.8
Wind direction	13.5
Conductor diameter	13.0
Phase clearance	11.3

IV. LEARNING ALGORITHMS AND PERFORMANCE EVALUATION

The utilized algorithms for creating the surrogate model that quantifies the conductor clashing risk score of each power line are discussed here. The features introduced in the previous section are fed into various supervised learning models to predict the clashing score as defined previously. The performance of five machine learning algorithms is compared based on the loss functions defined in Table III to find the optimal algorithm. Here, n is the total number of samples, y_i is the actual output value, and \hat{y}_i is the predicted output value. It is observed that for multiple linear regression (MLR), Random Forest Regression (RFR), and Deep Neural Network (DNN), the Mean Square Error (MSE) loss function is minimized. In the Least Absolute Shrinkage and Selection Operator (LASSO) regression cost function, the penalty factor $\lambda \|\theta\|_1$ is added to the cost function of MLR. It is an L_1 regularization penalty factor, where λ adjusts the improvement in error by varying the penalty magnitude, and it acts as a tuning parameter. In the Support Vector Regression (SVR) cost function, ω represents weight, b is the intercept, x_i is the i^{th} input feature, C represents the penalty factor, and ξ, ξ^* are slack variables.

Metrics for performance evaluation of learning algorithms such as mean absolute error (MAE), relative mean absolute error (r-MAE), root mean square error (RMSE), relative-root mean square error with mean (r-RMSE_m), and relative-root mean square error with maxmin (r-RMSE_{mm}) are expressed in Table IV.

TABLE III
THE LOSS FUNCTION OF VARIOUS LEARNING ALGORITHMS

Algorithm	Loss function
MLR, RFR, DNN	$\frac{1}{n} \sum_{i=1}^n (\hat{y}_i - y_i)^2$
LASSO	$\frac{1}{n} \sum_{i=1}^n (\hat{y}_i - y_i)^2 + \lambda \ \theta\ _1$
SVR	$\min_{\omega, b, \xi, \xi^*} \frac{1}{n} \ \omega\ _2^2 + C \sum_{i=1}^n (\xi_i + \xi_i^*)$

TABLE IV
PERFORMANCE EVALUATION METRICS FOR LEARNING ALGORITHMS

Metric	Formula
MAE	$\frac{1}{n} \sum_{i=1}^n \hat{y}_i - y_i $
r-MAE	$\frac{1}{n} \sum_{i=1}^n \hat{y}_i - y_i / \frac{1}{n} \sum_{i=1}^n y_i$
RMSE	$\sqrt{\frac{1}{n} \sum_{i=1}^n (\hat{y}_i - y_i)^2}$
r-RMSE _m	$\sqrt{\frac{1}{n} \sum_{i=1}^n (\hat{y}_i - y_i)^2 / \frac{1}{n} \sum_{i=1}^n y_i}$
r-RMSE _{mm}	$\sqrt{\frac{1}{n} \sum_{i=1}^n (\hat{y}_i - y_i)^2 / (y_{\max} - y_{\min})}$

V. SIMULATION RESULTS

In this section, the merit of the fire hazard risk scores and the performance of different learning models are discussed. The span of the power line, conductor diameter, wind speed, wind gust, phase clearance, and wind direction are considered as input features (x), where the predicted score is returned as output (y).

A. Comparison of Various Learning Algorithms

This section discusses the performance of different learning models, and the performance evaluation metrics described in Section IV are assessed for each model. To demonstrate the merit of the proposed surrogate model, the best performing model is selected, and it is compared with the Runge-Kutta method.

1) *MLR*: MLR models the relationship between input features and output score by fitting a linear equation to the observed data. Training of MLR model is performed based on the dataset, and the accuracy of clashing score predictions is evaluated. The value of α is equal to 0.0001. The metrics that show the best accuracy are MAE = 0.03, r-MAE = 0.96, RMSE = 0.05, r-RMSE_m = 1.37, and r-RMSE_{mm} = 0.11.

2) *LASSO*: For tuning, different values of λ are considered by varying it from 0-1. The performance evaluation metrics are calculated as shown in Table V. The result is the least-squares estimate when λ is 0. As λ increases, shrinkage occurs, and the variables that are zero can be discarded. The minimum value of evaluation metrics occurs when the penalty factor is $1e-4$, and it results in the same performance evaluation metrics as MLR. Results indicate that the inclusion of the penalty factor λ has a negative impact on the performance of the learning algorithm. Thus, all presented features are important to procure the score in the surrogate model, and no features should be left out of consideration.

TABLE V
TUNING OF LASSO REGRESSION BASED ON THE PENALTY FACTOR

λ	MAE	r-MAE	RMSE	r-RMSE _m	r-RMSE _{mm}
1e-4	0.03	0.96	0.05	1.37	0.11
1e-2	0.03	0.97	0.05	1.46	0.11
0.2	0.04	1.26	0.06	1.69	0.13
0.4	0.04	1.29	0.06	1.71	0.13
0.6	0.04	1.29	0.06	1.71	0.13
0.8	0.04	1.30	0.06	1.71	0.13
1.0	0.04	1.30	0.06	1.70	0.13

3) *SVR*: In SVR, hyper-parameter tuning is performed using ϵ and C. A sample of observations during parameter tuning is displayed in Table VI. It is observed that all errors are heavily penalized by setting $\epsilon = 0$ and C = 1.0, where the best performance is achieved. In this case, a high value of C indicates that more attention is paid to the loss caused by the outliers, and small ϵ shows that slack variables are in the dataset group.

TABLE VI
SVR PERFORMANCE FOR VARIOUS TUNING PARAMETERS

ϵ	C	MAE	r-MAE	RMSE	r-RMSE _m	r-RMSE _{mm}
0	0.5	0.02	0.65	0.04	1.26	0.10
0.2	0.5	0.11	3.15	0.12	3.34	0.27
0.4	0.5	0.05	1.58	0.07	1.95	0.15
0.6	1.0	0.03	1.00	0.07	1.99	0.16
0.8	1.0	0.03	1.00	0.07	1.99	0.16
1.0	1.0	0.03	1.00	0.07	1.99	0.16
0	1.0	0.02	0.64	0.04	1.24	0.10

4) *Random Forest Regression*: In this algorithm, each decision tree predicts its output, and the final output is obtained by calculating the average output of all trees. Each decision tree has a high variance, but the resultant variance is low when combined in parallel. The tuning of random forest is performed by varying the number of trees from 10 to 100. As shown in Table VII, increasing the number of trees enhances the quality of the procured solution. The least evaluation metrics occur when 100 trees are considered for predicting the score. Since the training procedure takes place only once, we can afford the higher computation times due to more complex RFR structures.

TABLE VII
RANDOM FOREST PERFORMANCE FOR DIFFERENT TREE SIZES

Trees	MAE	r-MAE	RMSE	r-RMSE _m	r-RMSE _{mm}
10	6.1×10^{-6}	2×10^{-4}	10×10^{-5}	3.2×10^{-3}	3×10^{-4}
20	6.5×10^{-6}	2×10^{-4}	10×10^{-5}	2.7×10^{-3}	2×10^{-4}
40	6.8×10^{-6}	2×10^{-4}	10×10^{-5}	2.7×10^{-3}	2×10^{-4}
60	6.6×10^{-6}	2×10^{-4}	7.9×10^{-5}	2.1×10^{-3}	2×10^{-4}
80	6×10^{-6}	2×10^{-4}	8.2×10^{-5}	2.2×10^{-3}	2×10^{-4}
100	6×10^{-6}	2×10^{-4}	7.3×10^{-5}	2×10^{-3}	2×10^{-4}

5) *Deep Neural Network*: A multi-layer perceptron neural network is tuned using a different number of layers, batch sizes, and the number of epochs. The performance evaluation metrics calculated by varying the number of layers and keeping batch sizes and the number of epochs constant are shown in Table VIII. The input features are normalized using the

Gaussian distribution with zero mean and unit variance. The output layer consists of a single neuron, and it has Rectified Linear Unit (ReLU) activation function in its last layer to output the conductor clashing score. The batch size is 1000, and the number of epochs is set to 100. By increasing the number of layers, an improvement in prediction occurs up to 6 layers. Further increase in the number of layers decreases the performance due to the hierarchy of the dataset.

TABLE VIII
THE IMPACT OF NUMBER OF LAYERS ON THE DNN PERFORMANCE WITH BATCH SIZE OF 1000 AND 100 EPOCHS

Layers	2	4	6	8
MAE	1.6×10^{-3}	0.3×10^{-3}	0.2×10^{-3}	40×10^{-3}
r-MAE	43×10^{-3}	9.1×10^{-3}	6.2×10^{-3}	12×10^{-3}
RMSE	2.5×10^{-3}	0.8×10^{-3}	0.6×10^{-3}	1.2×10^{-3}
r-RMSE _m	69×10^{-3}	22×10^{-3}	16×10^{-3}	35×10^{-3}
r-RMSE _{mm}	5.6×10^{-3}	1.8×10^{-3}	1.3×10^{-3}	2.8×10^{-3}

Next, we aim to obtain the optimal batch size value by changing the batch size and keeping six layers and 100 epochs. The performance evolution metrics calculated during the tuning process are shown in Table IX. The performance evaluation metrics decrease up to 512 batch size, but further increase in batch size increases the evaluation metrics. The smaller batch size results in a less accurate estimate of the gradient. Thus, 512 is the optimal batch size that can be propagated through the neural network.

TABLE IX
THE IMPACT OF BATCH SIZE ON DNN PERFORMANCE WITH 6 LAYERS AND 100 EPOCHS

Batch Size	32	128	512	2048
MAE	0.7×10^{-3}	0.6×10^{-3}	0.4×10^{-3}	0.6×10^{-3}
r-MAE	20×10^{-3}	18×10^{-3}	12×10^{-3}	18×10^{-3}
RMSE	2.2×10^{-3}	1.1×10^{-3}	1.1×10^{-3}	1.5×10^{-3}
r-RMSE _m	62×10^{-3}	32×10^{-3}	31×10^{-3}	42×10^{-3}
r-RMSE _{mm}	5×10^{-3}	2.5×10^{-3}	2.5×10^{-3}	3.3×10^{-3}

The optimal value for the number of epochs is obtained by varying the number of epochs and keeping six layers and 512 batch size. It is shown in Table X that by the increasing number of epochs from 70 to 130, the evaluation metrics show a decreasing trend, where no significant improvement is observed in MAE and r-MAE indicators. Based on the above discussion, the best performance of DNN is achieved when hyper-parameters are set to 6 layers, 512 batch size, and 130 epochs.

TABLE X
THE IMPACT OF NUMBER OF EPOCHS ON DNN PERFORMANCE WITH 6 LAYERS AND BATCH SIZE OF 512

Epochs	70	90	110	130
MAE	0.5×10^{-3}	0.3×10^{-3}	0.3×10^{-3}	0.4×10^{-3}
r-MAE	14×10^{-3}	9.6×10^{-3}	10×10^{-3}	12×10^{-3}
RMSE	1.4×10^{-3}	1×10^{-3}	1.1×10^{-3}	0.8×10^{-3}
r-RMSE _m	39×10^{-3}	28×10^{-3}	32×10^{-3}	23×10^{-3}
r-RMSE _{mm}	3.1×10^{-3}	2.2×10^{-3}	2.5×10^{-3}	1.8×10^{-3}

6) *Selection of the Best Learning Model:* To determine the most accurate learning model, we compared the best results obtained by applying each learning model using the optimal hyper-parameters, where RFR results in a better performance than LR, LASSO, and SVR. The optimal performance metrics for each model are shown in Table XI. LASSO regression model is not performing better than MLR because all features are important for the learning process, and discarding a feature leads to poor performance. This is consistent with the feature importance analysis that deemed no input feature is negligible. The non-linear SVR model based on radial basis function kernel learns the model well and performs better than MLR and LASSO. The error evaluation metrics give the small error in RFR, and this model predicts with the highest accuracy. The performance of DNN is acceptable, but it is not better than RFR. The major features leading to the efficient performance of RFR are wind speed (27.3%), the span of power lines (20.9%), and wind gust (13.8%), as shown in Table II. These features efficiently and effectively represent the physical power line movement. Therefore, RFR can be substituted as a surrogate model to forecast the clashing score and can be incorporated into practical applications.

TABLE XI
COMPARISON OF DIFFERENT LEARNING ALGORITHMS

Measure	MLR	LASSO	SVR	RFR	DNN
MAE	0.03	0.03	0.02	0.006×10^{-3}	0.2×10^{-3}
r-MAE	0.96	1.04	0.64	0.16×10^{-3}	6.2×10^{-3}
RMSE	0.05	0.05	0.04	0.072×10^{-3}	0.6×10^{-3}
r-RMSE _m	1.37	1.52	1.24	1.96×10^{-3}	10×10^{-3}
r-RMSE _{mm}	0.11	0.12	0.10	0.15×10^{-3}	1.3×10^{-3}

B. Comparing the Surrogate Model with Nonlinear Displacement Equations

To illustrate the validity of the proposed surrogate model, a comparison between the scores predicted by the surrogate model versus the analytical ones obtained from the physical model is presented in Table XII, where different power line spans at varying wind speeds, wind gusts, phase clearances, and wind directions are considered. It is noticed that the predicted score is almost equal to the values obtained by the RK model in all instances. For example, in the second row, the score obtained by the nonlinear displacement model is 0.071429, and the surrogate model predicted score is 0.071428. The surrogate model predicts the score with 99.99% test accuracy, where 20% of instances are designated to the test dataset. Therefore, the proposed surrogate model is an accurate representation of the nonlinear conductor displacement method. Comparing the scores obtained by the surrogate model and the mathematical model validates its accuracy in several instances. By utilizing the presented surrogate model based on machine learning, risk scores are obtained instantly, and the high computation burden is no longer an issue. System operators can make informed decisions for PSPS by de-energizing power lines having ignition scores above a specific threshold.

TABLE XII
COMPARISON BETWEEN THE PREDICTIONS OF PHYSICAL AND SURROGATE MODELS

L_c (ft)	d (mm)	V_w (m/s)	V_g (m/s)	Phase clearance (ft)	Angle (°)	Score	
						RFR	RK
800	33.03	26	26	1.5	45	0.0714	0.0714
500	33.03	18	20	0.7	45	0.0857	0.0857
1000	33.03	30	28	0.7	315	0.1285	0.1285
400	33.03	26	14	0.9	315	0.1714	0.1714
300	33.03	30	30	0.5	315	0.4571	0.4571

C. Impact of Various Meteorological and Structural Features on the Conductor Clashing Score

In this section, the surrogate model predicts the clashing score by varying different input features. The conductor clashing scores for different line spans and wind speeds are shown in Fig. 2, where it is illustrated that the clashing scores will be different for various line spans at the same wind speed. Here, the conductor diameter, phase clearance, and angle are kept constant to investigate the effect of power line span and wind speed on the conductor clashing. The increase in wind speed and wind gust leads to an increase in the conductor clashing score. The conductors with a larger span have a lower conductor clashing score for the same wind speed and wind gust because a larger span means conductors are heavier and harder to move. It is noticed that the conductor clashing scores of lines with shorter spans drop with the increase in wind speed above a certain threshold. This is because lighter conductors of various phases will move together at higher wind speeds, reducing conductor clashing. Thus, simultaneous consideration of meteorological and structural features is necessary.

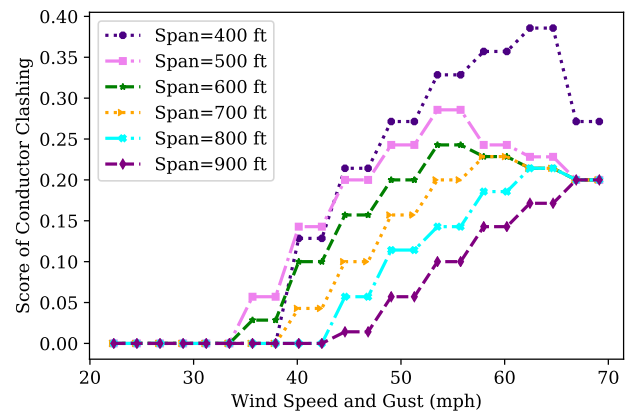


Fig. 2. Conductor clashing score for different spans using the surrogate model at $d=33.03$ mm, phase clearance=0.5 ft, and angle=45°

The conductor clashing scores for various phase clearances (PC) are shown in Fig. 3, where the span, diameter, and angle are set to 1000 ft, 33.03 mm, and 45°, respectively. A smaller phase clearance renders a higher clashing score. Based on this observation, it is concluded that choosing a one-size-fits-all threshold for wind speed (e.g., 50 mph) for line de-energizing is not a reliable approach.

When wind speed is constant, the conductor clashing score decreases with increasing phase clearances since. With a

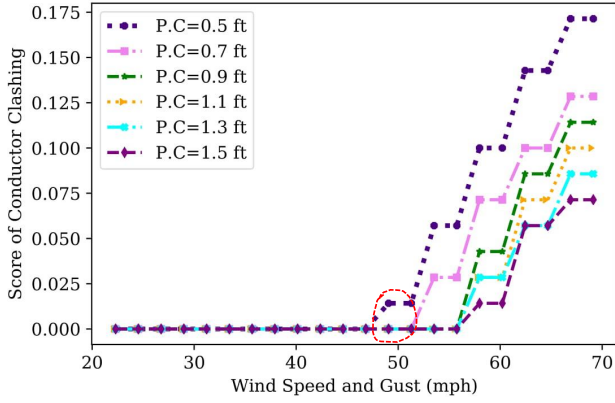


Fig. 3. Conductor clashing score for different phase clearances using the surrogate model at span=1000 ft, $d=33.03$ mm, and angle=45°

large phase clearance, the conductors move further apart, and smaller sections of the conductors will slap each other.

D. Demonstration of WRAP on 6-Bus System

In this section, two wind regimes are applied to a 6-bus test case system to illustrate the effectiveness of the proposed surrogate model to quantify the risk of wildfire for each power line. Thus, system operators will balance between the de-energizing of lines given the wildfire risk and the penalty for shedding the demand. On the one hand, the wildfire risk is reduced by de-energizing more power lines leading to a larger load shedding. On the other hand, keeping the power lines energized will serve the demand but results in a greater risk of wildfire ignition. Therefore, the risk and load shedding are balanced when a certain portion of the demand is enforced to serve. The wind direction and speed are represented by colored arrows, where the respective wind speed range to each color is shown in the legend. It is observed that the wind direction impacts most of the lines at an angle of 45°.

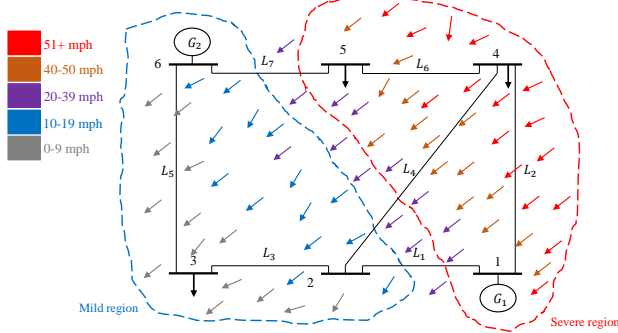


Fig. 4. Demonstration of wind impact on a 6-bus system

As a result of a higher wind speed within the severe region, lines L_2 , L_4 , and L_6 should be de-energized to avoid the risk of wildfire. The impact of wind speed decreases in orders of magnitude as the wind enters further inside the network in the mild region. Thus, lines L_1 , L_3 , L_5 , and L_7 , located within the mild region with a low wind speed, can reliably remain energized. The presented surrogate model enables system operators with a tool to decide on the de-energization of lines based on rendered fire hazard risk scores and risk tolerance and load continuity priority.

An analysis of the trade-off between load shedding and fire hazard risk by varying the load-serving percentage is presented in Fig. 5, where various values for the load-serving percentage, α in the WRAP formulation, are evaluated. With the change in the enforced load-serving from 0 to 100%, load shedding decreases from 3800 MWh to 0 MWh, and cumulative fire hazard risk increases from 0 to 9.4. The increase in the load-serving percentage leads an increase in objective cost from \$1.5 million to \$12.4 billion, which signifies the inherent cost of fire hazard risk. It is interesting to observe that by increasing load-serving percentage from 10% to 40%, the load shedding and cumulative score do not change. This is because the lines that were energized to serve the 10% of demand can still support the 40% of demand without needing additional support. Therefore, the fire hazard risk taken into account to serve the load remains unchanged.

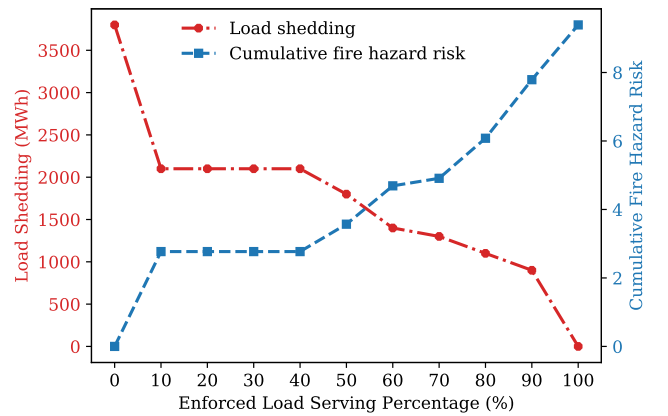


Fig. 5. The balance between load shedding and cumulative fire hazard risk based on enforced load serving in 6-bus system

E. Demonstration of WRAP on IEEE 30-Bus System

In this section, the presented surrogate model is applied to quantify the risk of wildfire ignition in modified IEEE 30-bus system during low and high wind speed situations. The network is overlaid on a similar geographical area where the meteorological information can be accessed at [35]. The available meteorological data includes wind speed, wind gust, and wind direction. Other structural features, including the span of line, conductor diameter, and phase clearance, are based on the data of the IEEE 30-bus system.

Assuming to serve all demand, the wildfire ignition score during low wind speed scenario is shown in Fig. 6. Here, the wildfire ignition score ranges between 0-0.06, with the majority of them being 0 due to low wind speed, with the maximum wind speed being 24 mph (11 m/s). The highest risk value of 0.06 belongs to the line connecting buses 6 and 8 because this region has the highest wind speed and gust of 24 mph, which lead to a relatively higher but still small fire hazard risk.

The wildfire ignition score during a high wind speed scenario is shown in Fig. 7. Here, the maximum wind speed reaches 62 mph (28 m/s), and the fire risk score ranges between 0 and 0.51, where the highest score is associated with the highest wind speed. The aggravating effect of higher wind speeds on ignition risk is noticeable in these two cases.

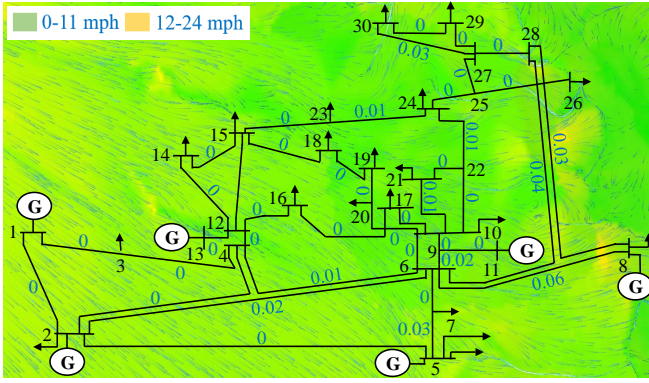


Fig. 6. The quantified risk of wildfire ignition for low wind speed case in the IEEE 30-bus system during 1st hour of the day

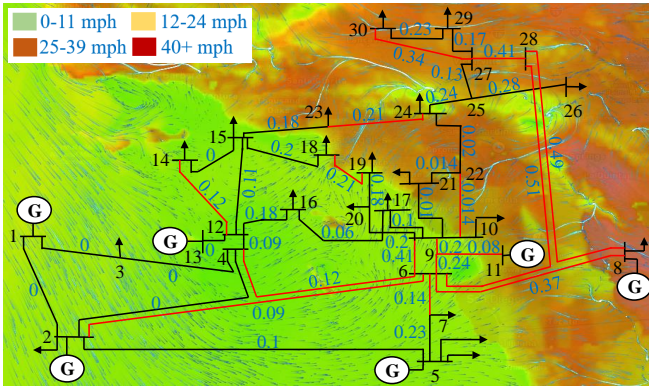


Fig. 7. The quantified risk of wildfire ignition for high wind speed case in the IEEE 30-bus system during 1st hour of the day

Although the peak wind speed here is only 2.5 times that in the low wind speed scenario, the maximum score in the high wind speed scenario is 8.5 times obtained in the low-speed scenario. The system operator may adjust the value of α to balance load-serving and the risk value. The presented WRAP model provides a tool for the system operator to balance fire hazard risk and service continuity leveraging the rendered risk score. As shown in Fig. 7 with $\alpha = 1$, several lines are de-energized by the system operator to mitigate the fire hazard risk and serve all of the demand simultaneously. It is noticed that in this case, the lines with higher risk scores are not necessarily de-energized. For example, the line connecting buses 5 and 7 (with a score of 0.23) is kept energized due to load-serving concerns. In contrast, the line connecting buses 2 and 6 (with a score of 0.09) is de-energized since its energization is not crucial to the system operation at this snapshot.

The balance between fire hazard risk and load shedding based on the percentage of forced load-serving is presented in Fig. 8. In the low wind scenario, at 0% enforced load serving, the objective cost is \$365,508 with the load shedding of 907 MWh and the cumulative fire hazard risk of 0. With the increase in the enforced load-serving percentage, load shedding is decreased while the fire risk hazard score is increased. It is observed that with the increase of the enforced load-serving from 0% to 10%, load shedding significantly drops to 0 MWh while the fire risk hazard is increased to 0.33. With 100% enforced load serving, the cumulative fire hazard risk is only 0.33 for the 24 hours of operation. The

system operator challenge to balance service continuity with load-serving is more complicated during the high wind speed scenario, as shown in Fig. 8, where the objective cost is \$2.12M and load shedding is 5200 MWh at 0% load serving. The reason behind the difference in MWh of load shedding in these two scenarios is the difference in the number of lines with a risk score of 0. By increasing the enforced load-serving from 10% to 40%, similar to what was observed in the 6-bus system case, the load shedding and cumulative fire hazard risk remain constant. It is noticed that the fire hazard risk in high wind scenarios sharply escalates when the system is forced to serve the first 10% of the demand, while no further sudden surges are observed as the percentage of the served load is increased, and the load shedding is decreased. This can be associated with the network structure, where to serve an even low percentage of the load, several lines must become energized. With the 100% enforced load serving, the objective cost is increased to \$152B, and the fire hazard score is increased to 95.2 for the 24 hours of operation.

The procured objective costs in these cases depend on the choice of the value of the penalty factor K , which tends to monetize the fire damage correlated with the risk of keeping a line energized. This value differs based on the area covered by the grid. Nevertheless, an investigation is presented here to figure out the sensitive number of hours-lines to the value choice for K , as shown in Fig. 9. With a very small choice of K , more lines will remain energized. However, the line energization is insensitive to the changes in K from 10^3 to 10^{10} , where $K = 10^4$ is employed in this case.

VI. CONCLUSIONS

This paper introduced a machine-learning-based surrogate model to quantify the risk of wildfire ignition by power lines under different weather conditions. The surrogate model is learned, predicting the ignition risk of power lines instantly and with high accuracy. It is interesting to observe that the presented surrogate model quantifies the risk of wildfire ignition with similar performance compared to the physical model. We also introduced the wildfire risk-aware operational planning model, which enables system operators to decide on the energization/de-energization of power lines based on a

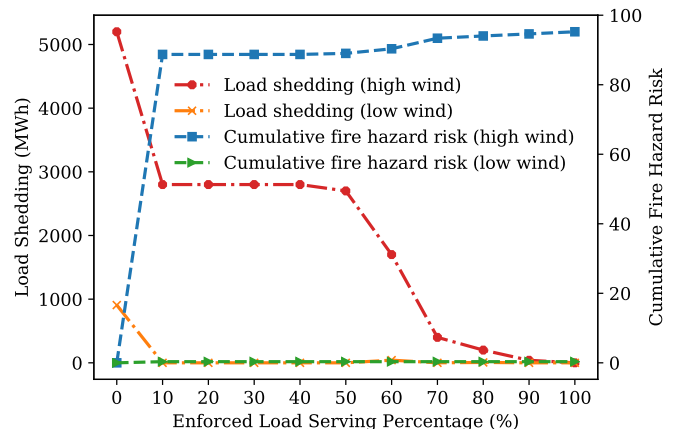


Fig. 8. The balance between load shedding and cumulative fire hazard risk based on enforced load serving in IEEE 30-bus system

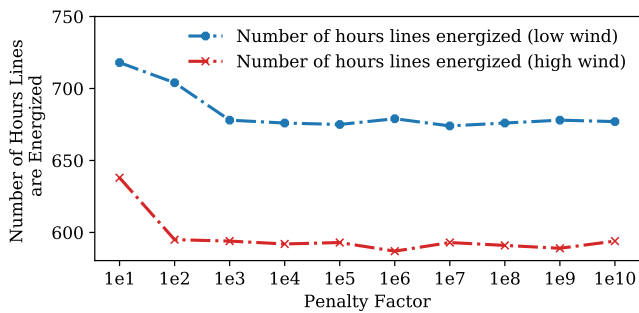


Fig. 9. Sensitivity of lines energization to penalty factor in the IEEE 30-bus system

quantified measure so that they can balance service continuity and wildfire safety. The presented model not only accounts for ignition risk during extreme weather conditions but also incorporates parameters that reflect the costs of potential wildfires while controlling the percentage of load that must be served. Interestingly, when a small portion of the load is enforced to serve, the cumulative fire hazard risk will experience a sharp increase. However, the risk will not significantly increase until a larger portion of demand is enforced to serve. With the geographical data availability, this tool can be applied to instantaneously pinpoint the power lines that need to be de-energized by system operators during *public safety power shut-off* events while allowing flexible decision-making.

REFERENCES

- [1] W. M. Jolly, M. A. Cochrane, P. H. Freeborn, Z. A. Holden, T. J. Brown, G. J. Williamson, and D. M. Bowman, "Climate-induced variations in global wildfire danger from 1979 to 2013," *Nature Communications*, vol. 6, no. 1, pp. 1–11, 2015.
- [2] K. T. Weber and R. Yadav, "Spatiotemporal trends in wildfires across the western united states (1950–2019)," *Remote Sensing*, vol. 12, no. 18, p. 2959, 2020.
- [3] D. Wang, D. Guan, S. Zhu, M. Mac Kinnon, G. Geng, Q. Zhang, H. Zheng, T. Lei, S. Shao, P. Gong *et al.*, "Economic footprint of California wildfires in 2018," *Nature Sustainability*, pp. 1–9, 2020.
- [4] California Public Utilities Commission, "Public safety power shutoff (PSPS) / de-energization," Available Online: <https://bit.ly/3AAhQ3e>, 2020.
- [5] Pacific Gas and Electric Company, "Pacific Gas and Electric Company amended 2019 wildfire safety plan," Available Online: <https://bit.ly/36d30Si>, 2019.
- [6] J. W. Mitchell, "Power line failures and catastrophic wildfires under extreme weather conditions," *Engineering Failure Analysis*, vol. 35, pp. 726–735, 2013.
- [7] A. D. Syphard and J. E. Keeley, "Location, timing and extent of wildfire vary by cause of ignition," *International Journal of Wildland Fire*, vol. 24, no. 1, pp. 37–47, 2015.
- [8] M. Sotolongo, C. Bolon, and S. H. Baker, "California power shutoffs: Deficiencies in data and reporting," in *Initiative for energy justice*, 2020. [Online]. Available: <https://bit.ly/3wfPibX>
- [9] T. Zhou, B. Li, C. Wu, Y. Tan, L. Mao, and W. Wu, "Studies on big data mining techniques in wildfire prevention for power system," in *2019 IEEE 3rd Conference on Energy Internet and Energy System Integration (EI2)*. IEEE, 2019, pp. 866–871.
- [10] J. P. Gentle, "Concurrent wind cooling in power transmission lines," Idaho National Laboratory (INL), Tech. Rep., 2012.
- [11] L. Lihong, H. Yi, L. Jinglu, and Z. Xiangjun, "Parameters for wind caused overhead transmission line swing and fault," in *TENCON 2006-IEEE Region 10 Conference*. IEEE, 2006, pp. 1–4.
- [12] E. Sutlovic, I. Ramljak, and M. Majstrovic, "Analysis of conductor clashing experiments," *Electrical Engineering*, vol. 101, no. 2, pp. 467–476, 2019.
- [13] S. Jazebi, F. De Leon, and A. Nelson, "Review of wildfire management techniques—part I: Causes, prevention, detection, suppression, and data analytics," *IEEE Transactions on Power Delivery*, vol. 35, no. 1, pp. 430–439, 2019.
- [14] C. Benner, B. Russell, J. Wischkaemper, K. Muthu-Manivannan, and R. Taylor, "DFA technology detects circuit device failures—experience of mid-south synergy," in *72nd Annual Conference for Protective Relay Engineers*, 2019.
- [15] B. D. Russell, C. L. Benner, and J. A. Wischkaemper, "Distribution feeder caused wildfires: Mechanisms and prevention," in *2012 65th Annual Conference for Protective Relay Engineers*. IEEE, 2012, pp. 43–51.
- [16] W. Ekard, T. Harold, and L. Rone, "2007 San Diego county firestorms after action fire report." EG&G Technical Services, Inc, 2007. [Online]. Available: <https://bit.ly/3wfBduY>
- [17] P. Murphy, "Preventing wildfires with power outages: the growing impacts of California's public safety power shutoffs," in *Energy and Environment Program*, 2021. [Online]. Available: <https://bit.ly/3hD26DX>
- [18] P. Stevens, "PG&E power outage could cost the California economy more than \$2 billion." CNBC, 2021. [Online]. Available: <https://cnb.cx/36e21kR>
- [19] M. Philips, "Oxygen-dependent California man dies 12 minutes after PG&E cuts power to his home." Fox News, 2021. [Online]. Available: <https://fxn.ws/3hKcGK>
- [20] T. O. Seppa, E. Cromer, and W. F. Whitlatch, "Summer thermal capabilities of transmission lines in Northern California based on a comprehensive study of wind conditions," *IEEE Transactions on Power Delivery*, vol. 8, no. 3, pp. 1551–1561, 1993.
- [21] M. Belloli, S. Melzi, S. Negrini, and G. Squicciarini, "Numerical analysis of the dynamic response of a 5-conductor expanded bundle subjected to turbulent wind," *IEEE Transactions on Power Delivery*, vol. 25, no. 4, pp. 3105–3112, 2010.
- [22] H. Volpe, "Bonneville power administration study of wind effects on conductors for span factors," vol. 7, no. 3, pp. 1387–1395, 1992.
- [23] D. Zhu, D. Cheng, R. P. Broadwater, and C. Scirbona, "Storm modeling for prediction of power distribution system outages," *Electric Power Systems Research*, vol. 77, no. 8, pp. 973–979, 2007.
- [24] Y. Guo, R. Chen, J. Shi, J. Wan, H. Yi, and J. Zhong, "Determination of the power transmission line ageing failure probability due to the impact of forest fire," *IET Generation, Transmission & Distribution*, vol. 12, no. 16, pp. 3812–3819, 2018.
- [25] M. Waseem and S. D. Manshadi, "Electricity grid resilience amid various natural disasters: Challenges and solutions," *The Electricity Journal*, vol. 33, no. 10, p. 106864, 2020.
- [26] J. W. Muhs, M. Parvania, and M. Shahidepour, "Wildfire risk mitigation: A paradigm shift in power systems planning and operation," *IEEE Open Access Journal of Power and Energy*, vol. 7, pp. 366–375, 2020.
- [27] F. Teng, "Enhancing power distribution grid resilience against massive wildfires," Ph.D. dissertation, The George Washington University, 2020.
- [28] N. Rhodes, L. Ntamo, and L. Roald, "Balancing wildfire risk and power outages through optimized power shut-offs," *arXiv preprint arXiv:2004.07156*, 2020.
- [29] S. Kandanaarachchi, N. Anantharama, and M. A. Munoz, "Early detection of vegetation ignition due to powerline faults," *IEEE Transactions on Power Delivery*, 2020.
- [30] J. Muhs, M. Parvania, H. T. Nguyen, and J. A. Palmer, "Characterizing probability of wildfire ignition caused by power distribution lines," *IEEE Transactions on Power Delivery*, 2020.
- [31] A. Arab, A. Khodaei, R. Eskandarpour, M. P. Thompson, and Y. Wei, "Three lines of defense for wildfire risk management in electric power grids: A review," *IEEE Access*, 2021.
- [32] M. Zhang, G. Zhao, and J. Li, "Nonlinear dynamic analysis of high-voltage overhead transmission lines," *Shock and Vibration*, 2018.
- [33] D. Tan and Z. Chen, "On a general formula of fourth order Runge-Kutta method," *Journal of Mathematical Science & Mathematics Education*, vol. 7, no. 2, pp. 1–10, 2012.
- [34] C. A. Fletcher, "Computational Galerkin Methods." Springer, 1984.
- [35] "SDGE Weather Awareness System," last accessed 6 July 2021. [Online]. Available: <https://sdgeweather.com>